

# Effects of extended components of [O III] on the correlation between the [O III] luminosity and the power-law continuum luminosity for active galactic nuclei

Xue-Guang Zhang<sup>\*</sup>, Long-Long Feng

*Institute of Astronomy and Space Science, Sun Yat-Sen University, No. 135, Xingang Xi Road, Guangzhou, 510275, P. R. China*

## ABSTRACT

In this manuscript, we check the well-known correlation between [O III] luminosity and continuum luminosity ( $L_{[\text{O III}]} - L_{5100\text{\AA}}$ ) for AGN by a large sample of 1982 SDSS QSOs with  $z < 0.8$  and with high quality spectra. The strong correlation of  $L_{[\text{O III}]} - L_{5100\text{\AA}}$  can be found, similar as previous results for AGN. Moreover, among the 1982 QSOs, there are 708 QSOs with the [O III] $\lambda 5007\text{\AA}$  described by two components: one core component plus one extended component. Based on the luminosity from the core components ( $L_{[\text{O III}], \text{ narrow}}$ ) and from the extended components ( $L_{[\text{O III}], \text{ ext}}$ ), we confirm that the correlation of  $L_{[\text{O III}], \text{ ext}} - L_{5100\text{\AA}}$  is more stronger and tighter than the correlations on the total [O III] luminosity and on the luminosity of the core components of the [O III] lines. Therefore, the luminosity of the extended components should be better applied to trace AGN intrinsic luminosity. Meanwhile, we have found strong line width correlation and line luminosity correlation between the core components and the extended components, indicating the extended components of the [O III] lines should be not due to commonly considered radial flows in the common [O III] line clouds. And virial effects due to gravity of central black holes naturally lead to the wider extended components from regions more nearer to central black holes. Finally, we can say that the reported correlation of  $L_{[\text{O III}], \text{ narrow}} - L_{5100\text{\AA}}$  on the core components of the [O III] lines should be more better to estimate AGN intrinsic luminosity in Type-2 narrow line AGN, because of totally/partly obscured extended components.

**Key words:** galaxies:active - galaxies:nuclei - quasars:emission lines - galaxies:Seyfert

## 1 INTRODUCTION

The well-known constantly being revised Unified Model (UM) have been widely accepted to explain most of the different observed phenomena between broad line active galactic nuclei (Type-1 AGN) and narrow line AGN (Type-2 AGN), due to expected different orientation angles of the central accretion disk Antonucci (1993), combining with different central activity and different properties of the inner dust torus etc. (Marinucci et al. 2012; Oh et al. 2015; Mateos et al. 2016). The more recent review on the UM can be found in Bianchi et al. (2012) and in Netzer (2015). The UM simply indicates that Type-2 AGN are intrinsically like Type-1 AGN, but their central regions including broad line regions (BLRs) are hidden from our view by central dust torus and/or high density dust clouds, and the unobscured narrow emission lines can be well applied to trace the central region properties of Type-2 AGN. Strong [O III] emission lines coming from NLRs can be treated as one of the fundamental characteristics of AGN, and [O III] line luminosity is arguably the best available substitute for AGN intrinsic luminosity which have been studied, proved and reported in Simpson (1998);

Kauffmann et al. (2003); Zakamska et al. (2003); Heckman et al. (2005); Netzer et al. (2006); Reyes et al. (2008); Lamasra et al. (2009); Trouille & Barger (2010); Stern & Laor (2012); Shao et al. (2013); Heckman & Best (2014); Berney et al. (2015); Ueda et al. (2015), etc., although scatters may be a bit large for the correlations between the [O III] luminosity and the continuum luminosity (optical band, Infrared Radiation band or X-ray band luminosity, etc.). Therefore, even in Type-2 AGN with central regions totally obscured by dust torus (no observed optical broad emission lines in observed spectra), the [O III] line luminosity can be commonly applied to estimate AGN luminosity.

Besides the strong connection between the [O III] line luminosity and the AGN continuum luminosity, we can also notice that NLRs can be directly spatially resolved in nearby AGN, due to long distances of NLRs to central black holes and very extended structures of NLRs, such as the results based on high-quality images in Bennert et al. (2002); Schmitt et al. (2003); Bennert et al. (2006); Greene et al. (2011); Hainline et al. (2013); Liu et al. (2013); Fischer et al. (2013); Hainline et al. (2014); Liu et al. (2014). The distances of NLRs to central black holes (NLRs sizes) can be estimated by the [O III] line luminosity, leading to the result that the AGN NLRs sizes (tens of pcs to thousands of pcs) are more longer

\* Corresponding author Email: zhangxg23@sysu.edu.cn

than the AGN BLRs sizes (commonly several light-days to several hundreds of light-days, such as the more recent results in [Bentz et al. \(2013\)](#)), leading to a vast space between the NLRs and the BLRs. And since the first oversimplified results on properties of the vast space in [Netzer & Laor \(1993\)](#) based on expected dusts in NLRs, there is so far no clear and confirmed information on materials and corresponding dynamic structures in the space between the NLRs and the BLRs in AGN.

Meanwhile, based on profile properties of [O III] emission lines, part of AGN have their observed [O III] lines with much extended wings, such as the well shown results in [Greene & Ho \(2005\)](#). Meanwhile, there are many studies on the shifted extended components in the [O III] emission lines. [Heckman et al. \(1981\)](#) have suggested dust and gas radial flows in narrow line regions with respect to the nucleus, in order to well explain the asymmetry of [O III] line due to the extended wings. [Nelson & Whittle \(1996\)](#) have found moderately strong correlation between stellar velocity dispersions and widths of the core components of [O III] emission lines but more weaker correlation with widths of the extended wings of [O III] emission lines. [Mullaney et al. \(2013\)](#) have suggested that outflowing components could lead to blue-shifted extended wings of [O III] emission lines especially in Type-1 AGN. [Zakamska & Greene \(2014\)](#) have reported evidence on outflows ultimately driven by the radiative output of the quasars, based on studies of shifted extended components of [O III] emission lines. [Woo et al. \(2016\)](#) have suggested that the extended wings of [O III] emission lines (probable from outflows) should be a component not dominated by the bulge gravitational potential.

Although there is so far no clear evidence on the physical origin of the extended wings of the [O III] lines, we can expect that the extended wings of the [O III] lines should be more nearer to central regions due to their larger line widths, and perhaps properties of the extended wings could provide some information on materials in the vast space between the NLRs and the BLRs. Therefore, it is interesting to check properties of the extended wings of the [O III] lines, through the reported correlation between the [O III] line luminosity and the AGN continuum luminosity after considerations of contributions of the extended wings. In this manuscript, we analyze properties of the [O III] emission lines for a large sample of QSOs with high quality spectra. And the manuscript is organized as follows. In Section 2, we show our main data sample. In Section 3, we show our main results and necessary discussions. Then, in Section 4, we give our final conclusions. And in this manuscript, the cosmological parameters of  $H_0 = 70 \text{ km} \cdot \text{s}^{-1} \text{ Mpc}^{-1}$ ,  $\Omega_\Lambda = 0.7$  and  $\Omega_m = 0.3$  have been adopted.

## 2 DATA SAMPLE

In this manuscript, we consider all QSOs with absolute magnitudes at i band smaller than -22.0 and with at least one emission line having width larger than 1000 km/s (see more detailed techniques discussed in [Schneider et al. \(2010\)](#)) in more recent Sloan Digital Sky Survey, Data Release 12 (SDSS DR12, [Alam et al. \(2015\)](#)) by the following two criteria: redshift  $z < 0.8$  to ensure [O III] lines included in SDSS spectra and mean signal-to-noise at g-band and at r-band larger than 20 to ensure high quality spectra around [O III] emission lines. Here, the convenient Structured Query Language (SQL) queries run from SDSS DR12 SkyServer search tools ([skyserver.sdss.org/dr12/en/tools/search/sql.aspx](http://skyserver.sdss.org/dr12/en/tools/search/sql.aspx)) by keywords of INSTRUMENT = 'SDSS', class = 'QSO',  $z < 0.8$  and  $z_{\text{warning}}=0$ ,  $\text{snMedian}_g > 20$  and  $\text{snMedian}_r > 20$

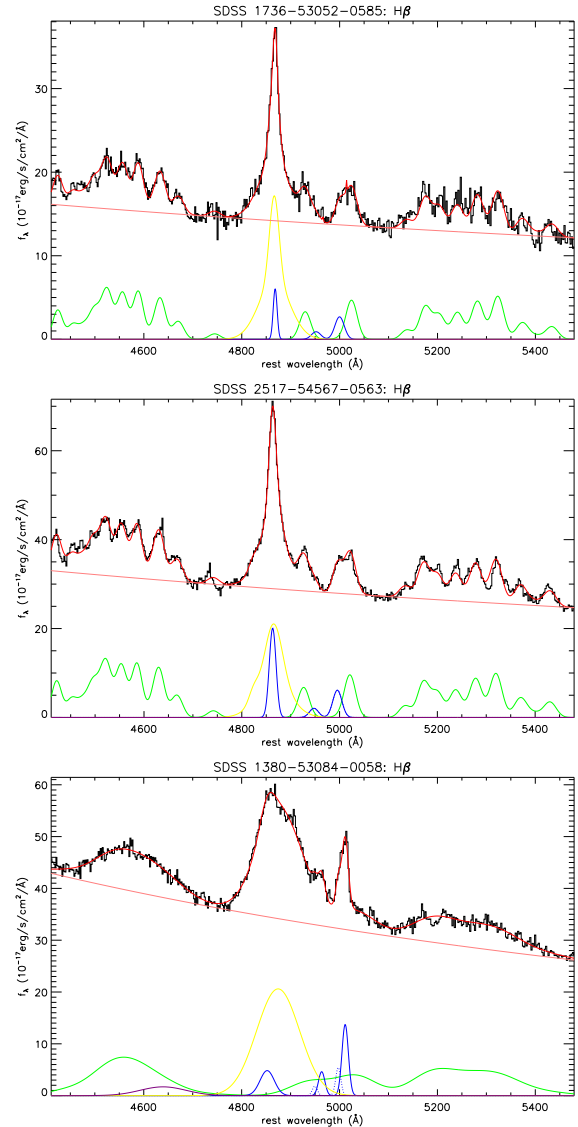


**Figure 1.** Best fitted results to the emission lines around H $\beta$  in SDSS 1736-53052-0585, 2517-54567-0563 and 1380-53084-0058, respectively. In each panel, solid lines in black, in red, in pink, in yellow, in blue and in green show the observed spectra, the best fitted results, the determined power-law continuum emissions, the determined broad H $\beta$ , the determined narrow H $\beta$  plus the narrow [O III] lines and the determined optical Fe II lines, respectively. In bottom panel for SDSS 1380-53084-0058, dotted line in blue shows the determined extended wings of the [O III] doublet, and solid line in purple shows the determined broad He II line.

from SDSS datatable of 'specobjALL'. Based on the criteria, there are 2820 QSOs selected from SDSS DR12. Then, emission line parameters and continuum emissions for each QSO can be measured from the SDSS spectrum as follows. Here, in this manuscript, [O III] lines are mainly focused on.

For the emission lines around H $\beta$  with rest wavelength from 4300Å to 5600Å: broad and narrow H $\beta$ , [O III] doublet, He II line and probable optical Fe II lines, the following model functions and Fe II templates are applied. Three (or more if necessary) broad Gaussian functions are applied to the broad H $\beta$ , one narrow Gaussian function is applied to the narrow H $\beta$ , one broad Gaussian function is applied to the probable He II line, two narrow Gaussian func-

tions are applied to the [O III] doublet and two other Gaussian functions are applied to the probable extended components of the [O III] doublet. And the more recent discussed Fe II template in Kovacevic et al. (2010) is applied to describe the optical Fe II lines. And a power-law function is applied to describe the AGN continuum emissions underneath the emission lines. Moreover, when the model functions and the Fe II template are applied, besides limitation of the same redshift to the narrow lines, no further restrictions are applied. In other words, it is allowed to have a bit different widths of the narrow H $\beta$  and the narrow [O III] doublet. Here, a broad Gaussian function means the function with second moment no smaller than 800 km/s. and a narrow Gaussian function means the function with second moment no larger than 600 km/s. The much similar emission line fitting procedure can also be found in our more recent paper in Zhang & Feng (2016).

Then, through the Levenberg-Marquardt least-squares minimization technique, emission lines can be well fitted, and basic parameters and corresponding uncertainties can be well determined. Then, we check the fitted results for the emission lines of the selected 2820 QSOs by eyes. And 838 objects are rejected, due to loss of [O III] lines (many bad pixels around [O III] or no detected apparent [O III] lines). Finally, there are 1982 QSOs with blue spectra and measured line parameters at least three times larger than their corresponding uncertainties included in our final main sample. Here, we do not show the best fitted results to the emission lines for all the selected QSOs, but Fig. 1 shows three examples on the best fitted results to the emission lines in SDSS 1736-53052-0585, 2517-54567-0563 and 1380-53084-0058 (PLATE-MJD-FIBERID), respectively. In SDSS 1736-53052-0585 and SDSS 2517-54567-0563, one Gaussian component is enough to describe the [O III] $\lambda$ 5007Å line, but in SDSS 1380-53084-0058, two components are necessary to well describe the [O III] $\lambda$ 5007Å line.

Before proceeding further to check the expected correlation between the [O III] luminosity and the AGN continuum luminosity, it is necessary to ensure whether our measured parameters (especially the [O III] luminosity including contributions of the extended wings and continuum luminosity) are reliable. We can find that among the 1982 QSOs in our main sample, 810 QSOs can also be found in the sample of Shen et al. (2011). Then, we compare our measured parameters (the total [O III] luminosity  $L_{[\text{O III}]}$  and continuum luminosity  $L_{5100\text{\AA}}$ ) with the reported values of  $L_{[\text{O III}], S11}$  and  $L_{5100\text{\AA}, S11}$  of the 810 QSOs in Shen et al. (2011). Fig. 2 shows the comparisons between our values and the values in Shen et al. (2011). Similar results can be confirmed between our measured parameters and the reported values in Shen et al. (2011), except about three outliers marked by solid circles in red in Fig. 2. However, we have checked our fitted results for the three outliers which have been shown in Fig. 1, and found our parameters should be better. We do not know the clear reasons to the different [O III] and/or continuum luminosities from them reported in Shen et al. (2011) for the three outliers. The main difference of the fitting procedures in Shen et al. (2011) and in the manuscript is the different optical Fe II template applied. Shen et al. (2011) have accepted the Fe II template discussed in Boroson & Green (1992). In our fitting procedure, the Fe II template discussed in Kovacevic et al. (2010) have been accepted. However, the different Fe II templates should not lead to different continuum emissions at 5100Å or different [O III] luminosity. The results shown in Fig. 2 indicate our measured [O III] and continuum luminosities are reliable.

Finally, based on the high quality SDSS spectra and the measured parameters, there are 1982 blue QSOs with the reliable line

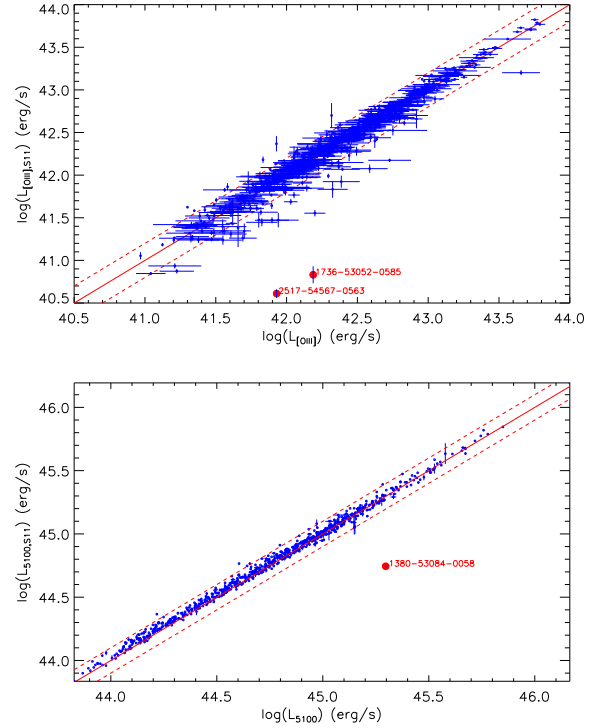


**Figure 2.** Comparisons of the total [O III] luminosity (top panel) and the continuum luminosity (bottom panel) at 5100Å between our measured parameters and the reported values in Shen et al. (2011). In top panel, solid line in red and dashed lines in red show  $\log(L_{[\text{O III}]} = \log(L_{[\text{O III}], S11})$  and its corresponding scatter of 0.2dex. Red circles show the two outliers away from the linear correlation, of which the best fitted results to the emission lines are shown in the top panel and the middle panel of Fig. 1. In bottom panel, solid line in red and dashed lines in red show  $\log(L_{5100\text{\AA}} = \log(L_{5100\text{\AA}, S11})$  and its corresponding scatter of 0.1dex. Red circle shows the outlier away from the linear correlation, of which the best fitted results to the emission lines are shown in the bottom panel of Fig. 1.

parameters of the [O III] lines and the reliable measured continuum luminosity in our final main sample. And based on the fitted results to the emission lines around H $\beta$ , there are 708 QSOs with their [O III] $\lambda$ 5007Å described by two reliable components of one core plus one extended wing. Then, we can check the contributions of the extended wings of the [O III] lines to the correlation between the [O III] luminosity and the continuum luminosity. Because of the large size of the data sample on the 1982 QSOs (or even for the 708 QSOs of which [O III] lines include extended wings), we do not list the basic parameters for all the QSOs in the manuscript. But, the basic parameters saved in FIT files and the best fitted results to the emission lines of the QSOs saved in EPS files can be downloaded from the website of <http://pan.baidu.com/s/1c1Nh1b6>.

### 3 MAIN RESULTS AND DISCUSSIONS

#### 3.1 Whether are the extended components of [O III] lines truly from [O III] emission clouds?

In order to confirm our following results on properties of different components of the [O III] emission lines, it is necessary to confirm whether are the determined extended components truly from [O III] clouds, not from the common broad emission line clouds (such

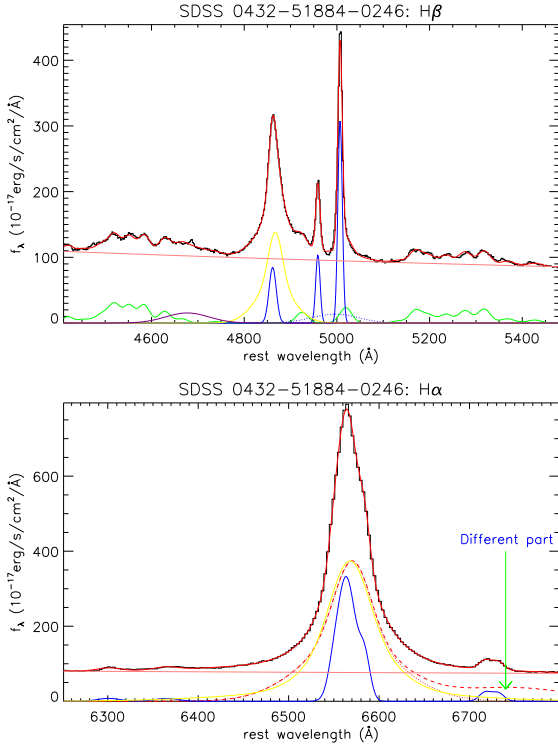


**Figure 3.** Emission lines and the best fitted results in SDSS 0432-51884-0246. Top panel shows the results on the emission lines around the  $H\beta$ . Symbols and lines have the same meanings as those shown in the bottom panel of Fig. 1. Bottom panel shows the results on the emission lines around the  $H\alpha$ . In bottom panel, solid lines in black, in red, in yellow, in blue and in pink show the observed spectrum, best fitted results to the lines, the determined broad  $H\alpha$ , the determined narrow lines and the determined power-law continuum, respectively. The dotted line in red shows the scaled and shifted broad  $H\beta$  component shown in yellow line in the top panel, with a scale factor of 2.7. And the dashed line in red shows the scaled and shifted components of the broad  $H\beta$  component shown in yellow line in the top panel plus the extended components shown in dotted line in blue in the top panel, with the same scale factor of 2.7. In bottom panel, the vertical line in green marks the position on the much different line profiles with and without contributions of the extended components of the [O III] doublet.

as, the extended components could be expected from broad  $H\beta$  line clouds). Here, two ways are applied to confirm the extended components are from [O III] clouds not from broad line clouds, based on the effects of the extended components on central wavelength and line width of the broad  $H\beta$ . On the one hand, we show an example to clearly declare the extended components are from [O III] clouds, no from broad  $H\beta$  clouds. Fig. 3 shows the emission lines and the fitted results in the object SDSS 0432-51884-0246, which has the second moment of the extended component of the [O III]  $\lambda 5007\text{\AA}$  larger than 2000 km/s. Then, based on the results shown in Fig. 3, we can find that if the extended components were from the broad  $H\beta$  clouds, there could be much different line profiles of the broad  $H\beta$  and the broad  $H\alpha$ : the solid line in yellow, the dotted line in red and the dashed line in red shown in the bottom panel of Fig. 3. In order to show more clearer effects of the extended components, we check central wavelengths of the broad  $H\beta$  with and without contributions of the extended components. Through the determined broad line profile without the contributions of the extended component, the central wavelength of the broad  $H\beta$  is about 4866Å. However, with considerations of the extended components to the broad  $H\beta$ , the

central wavelength should be about 4887Å. Meanwhile, the central wavelength of the broad  $H\alpha$  is about 6566Å, leading to the expected central wavelength of the broad  $H\beta$  of about 4865Å. Here, the central wavelengths are calculated by the definition shown in the following Equation (1). Therefore, under the accepted criterion that there are similar line profiles of the broad Balmer lines, the extended components are preferred from the [O III] clouds in SDSS 0432-51884-0246.

On the other hand, we check the central wavelength correlation and the broad line width correlation between the broad  $H\beta$  and the broad  $H\alpha$  for the 205 low redshift QSOs with both the broad  $H\beta$  and the broad  $H\alpha$  included in their SDSS spectra. Here, rather than the full width at half maximum (FWHM), the second moment is applied, because the extended components of the [O III] lines have more stronger effects on the second moment than on the FWHM. The second moment  $\sigma$  and the central wavelength  $\lambda_0$  are calculated by the line profiles through the definitions in Peterson et al. (2004),

$$\lambda_0 = \frac{\int \lambda \times P_\lambda d\lambda}{\int P_\lambda d\lambda}, \quad \sigma = \frac{\int \lambda^2 \times P_\lambda d\lambda}{\int P_\lambda d\lambda} - \lambda_0^2 \quad (1)$$

, where  $\lambda$  and  $P_\lambda$  represent the wavelength and the broad line profile, respectively. Here, the rest wavelength ranges from 4700Å to 5020Å and from 6400Å to 6720Å are applied to calculate the  $\sigma$  and the  $\lambda_0$  of the broad  $H\beta$  and the broad  $H\alpha$ , respectively. Then, two kinds of  $\sigma$  ( $\lambda_0$ ) are calculated for the broad  $H\beta$ , with and without contributions of the extended components of the [O III] lines.

Top panels of Fig. 4 show the two strong linear correlations for  $\sigma$  and  $\lambda_0$  determined from the pure broad components of the Balmer lines. The Spearman Rank correlation coefficients are 0.85 and 0.85 for the central wavelength correlation and for the broad line width correlation, respectively. And based on the more recent least trimmed squares robust (LTSR) technique (Cappellari et al. 2013) (the LTS\_LINEFIT code provided by Prof. Cappellari M., see also in <http://www-astro.physics.ox.ac.uk/~mxc/software>) with considerations of the uncertainties in both coordinates, the strong linear broad line width correlation can be described by

$$\log\left(\frac{\sigma_{H\beta}}{\text{km/s}}\right) = (0.66 \pm 0.09) + (0.79 \pm 0.03) \times \log\left(\frac{\sigma_{H\alpha}}{\text{km/s}}\right) \quad (2)$$

. And the central wavelengths of the broad  $H\alpha$  and the broad  $H\beta$  are well described by the expected relationship of  $\lambda_0(H\alpha) = \lambda_0(H\beta) \times \frac{6564.61}{4862.68}$  (where 6564.61Å and 4862.68Å are the theoretical central wavelengths of the  $H\alpha$  and the  $H\beta$ ). Then, bottom panels of Fig. 4 show the two loose correlations on the  $\sigma_{H\beta, \text{ext}}$  and the  $\lambda_0(H\beta, \text{ext})$  determined from the pure broad components of the  $H\beta$  plus the extended components of the [O III] lines, if we assumed that the extended components were from broad  $H\beta$  emission clouds. The Spearman Rank correlation coefficients are 0.22 and 0.49 for the central wavelength correlation and for the broad line width correlation, respectively. In other words, under assumptions that the extended components were from the broad  $H\beta$  emission clouds, there could be much different profiles of the broad  $H\beta$  and the broad  $H\alpha$ . Therefore, the results shown in Fig. 4 strongly support that the determined extended components are true components from the [O III] clouds not from the broad line clouds.

### 3.2 Main Results

Once we confirm the extended components are truly from the [O III] clouds, we can discuss our main results on the core and the extended components of the [O III] emission lines.

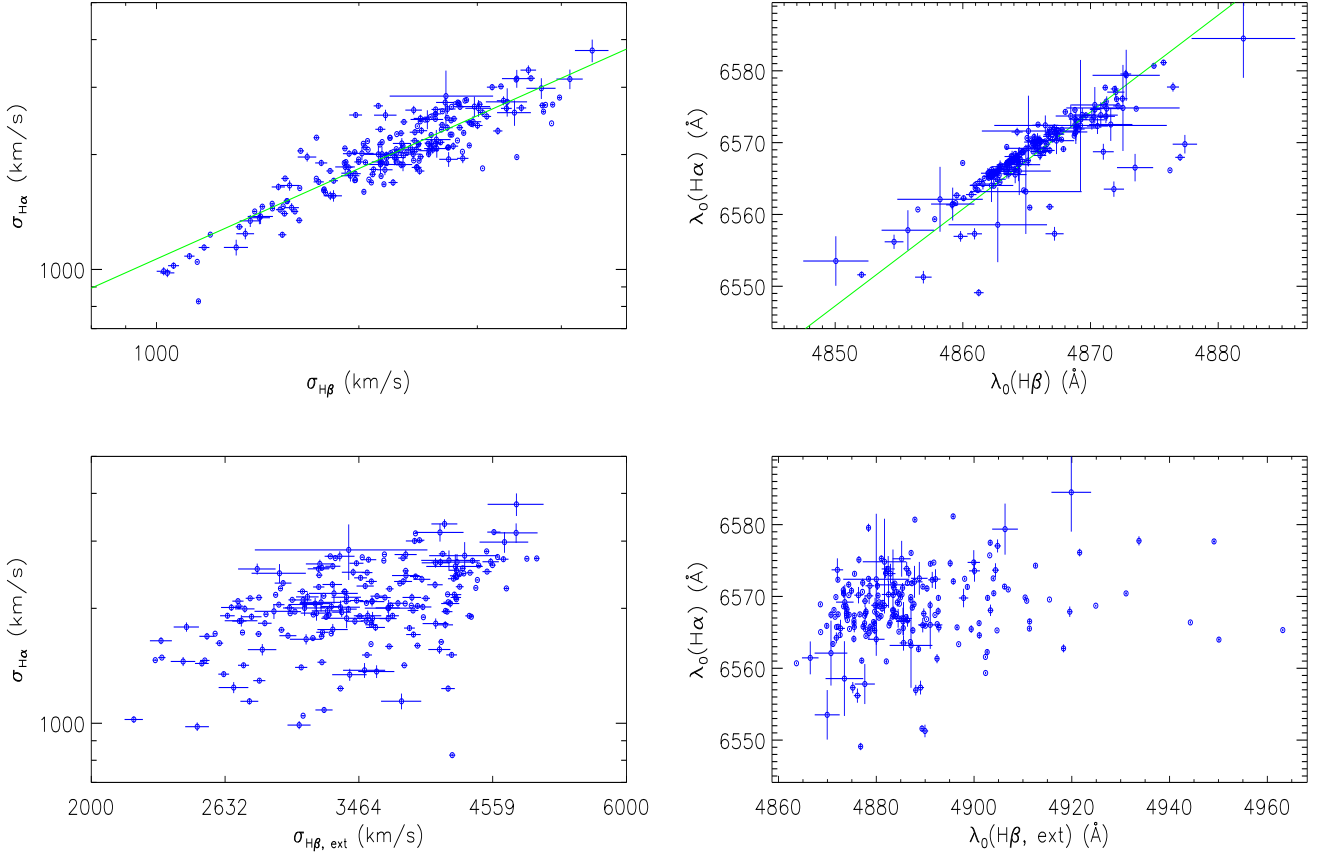


**Figure 4.** Broad line width correlation (left panels) and central wavelength correlation (right panels) of the broad Balmer lines for the low redshift QSOs. Top panels are the results on the profiles of the determined pure broad components of the Balmer lines, and bottom panels are on the results of  $\sigma_{H\beta, \text{ext}}$  and  $\lambda_0(H\beta, \text{ext})$  on the profiles of the determined pure broad components of the  $H\beta$  plus the extended components of the [O III] lines. In top left panel, solid line in green shows the best fitted result. In top right panel, solid line in green shows  $\lambda_0(H\alpha) = \lambda_0(H\beta) \times \frac{6564.61}{4862.68}$ .

We firstly check the correlation between the total [O III] luminosity and the continuum luminosity for our selected 1982 QSOs, which is shown in the top panel of Fig. 5. The strong linear correlation can be confirmed with the Spearman Rank correlation coefficient of about 0.79. And based on the more recent LTSR technique with considerations of the uncertainties in both coordinates, the strong linear correlation can be described by

$$\log\left(\frac{L_{5100\text{\AA}}}{\text{erg/s}}\right) = (12.43 \pm 0.51) + (0.764 \pm 0.012) \times \log\left(\frac{L_{[\text{O III}]}}{\text{erg/s}}\right) \quad (3)$$

. And the mean ratio of the continuum luminosity to the total [O III] luminosity is about 411. The strong linear correlation not only re-declares that the [O III] luminosity can be well applied to traced the AGN intrinsic luminosity similar as previous reported results, but also re-confirms that our measured parameters are reliable. Here, in the top panel, we also show the previous reported results  $L_{5100\text{\AA}} \sim 321 \times L_{[\text{O III}]}$  in Heckman et al. (2004) and  $L_{[\text{O III}]} \propto L_{5100\text{\AA}}^\beta$  with  $\beta = 0.77, 1.34$  by different fitting methods in Shen et al. (2011).

Then, we can check the correlations between the continuum luminosity and the luminosity from the two components of [O III] $\lambda 5007\text{\AA}$ . Here, a simple criterion is applied that the extended component is broader than the core component, to determine the extended component and the core component. Then, the correlations

are shown in the middle and the bottom panels of Fig. 5. There are also two strong linear correlations of  $L_{5100\text{\AA}}$  versus  $L_{[\text{O III}], \text{narrow}}$  (luminosity from the core components) and  $L_{5100\text{\AA}}$  versus  $L_{[\text{O III}], \text{ext}}$  (luminosity from the extended components), with the Spearman Rank correlation coefficients of about 0.71 and 0.86, respectively. And based on the more recent LTSR technique with considerations of the uncertainties in both coordinates, the strong linear correlations can be described by

$$\begin{aligned} \log\left(\frac{L_{5100\text{\AA}}}{\text{erg/s}}\right) &= (17.28 \pm 0.98) + \\ & (0.653 \pm 0.023) \times \log\left(\frac{L_{[\text{O III}], \text{narrow}}}{\text{erg/s}}\right) \\ \log\left(\frac{L_{5100\text{\AA}}}{\text{erg/s}}\right) &= (11.06 \pm 0.71) + \\ & (0.800 \pm 0.017) \times \log\left(\frac{L_{[\text{O III}], \text{ext}}}{\text{erg/s}}\right) \end{aligned} \quad (4)$$

. And the mean ratios of  $L_{5100\text{\AA}}$  to  $L_{[\text{O III}], \text{narrow}}$  and to  $L_{[\text{O III}], \text{ext}}$  are about 863 and 569, respectively. Therefore, we so far show the first report on the stronger linear correlation on the luminosity of the extended components of the [O III] lines.

Moreover, we have checked the improved quality on the extended components of the [O III] lines applied to trace the AGN

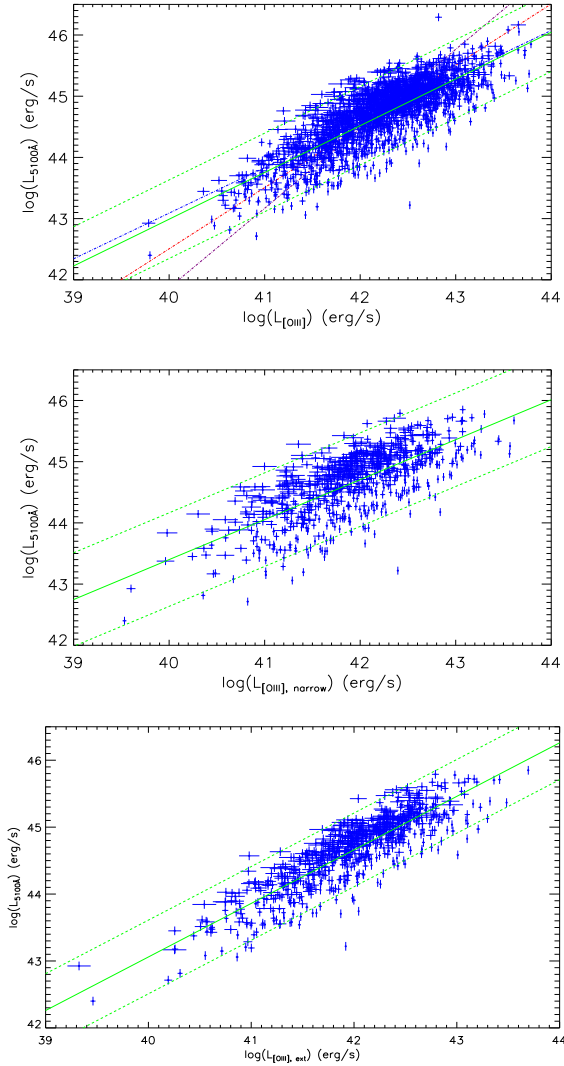


**Figure 5.** Correlations between the continuum luminosity and the [O III] luminosity. From top to bottom, the results are on the total [O III] luminosity, on the luminosity from the core components of the [O III] lines and on the luminosity from the extended components of the [O III] lines, respectively. In each panel, solid line in green shows the best fitted results, and dashed lines in green show the corresponding confidence levels of 95%. In top panel, the dot-dashed line represents the reported  $L_{5100\text{\AA}} \sim 321 \times L_{[\text{O III}]}$  in Heckman et al. (2004), and the dot-dashed lines in purple and in blue represent the fitted results by different methods reported in Shen et al. (2011).

intrinsic luminosity. In each panel of Fig. 5, we have shown the corresponding confidence levels of 95% for the best fitted result. And we can determine that the corresponding scatters are about 0.51dex, 0.64dex and 0.43dex for the correlations on the total [O III] luminosity, on the luminosity from the core components of the [O III] lines and on the luminosity from the extended components of the [O III] lines, respectively. Therefore, the luminosity of the extended components of the [O III] lines leads to more tighter linear correlation, which indicates the luminosity of the extended components of the [O III] lines should be a better indicator of AGN intrinsic luminosity, than both the total [O III] luminosity and the luminosity from the core components.

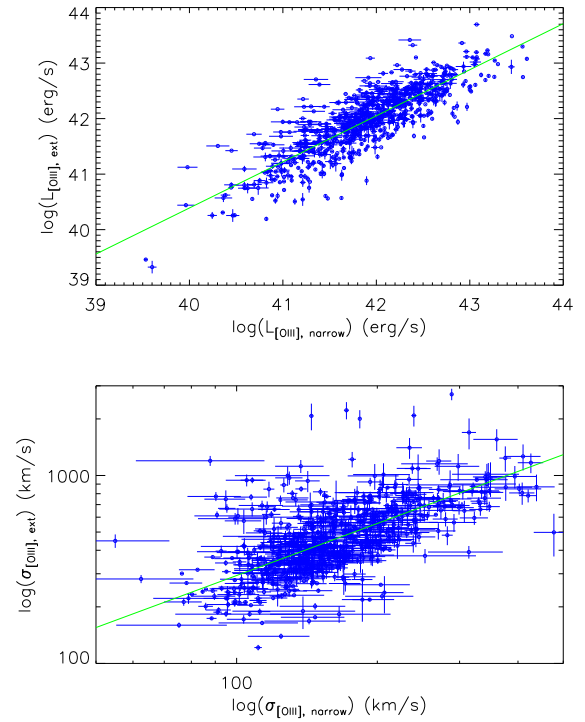


**Figure 6.** Luminosity correlation (top panel) and width correlation (bottom panel) between the core components and the extended components of the 708 QSOs with the [O III] lines including both the core components and the extended components. In each panel, solid line in green shows the best fitted result.

### 3.3 Main Discussions

First and foremost, we check the probable relationship between the core components and the extended components of the [O III] lines. Top panel of Fig. 6 shows the luminosity correlation between the core components and the extended components of the [O III] lines. There is one strong linear correlation with the Spearman Rank correlation coefficient of 0.83. And based on the more recent LTSR technique with considerations of the uncertainties in both coordinates, the strong linear correlation can be described by

$$\log\left(\frac{L_{[\text{O III}], \text{ext}}}{\text{erg/s}}\right) = (7.19 \pm 0.84) + (0.83 \pm 0.02) \times \log\left(\frac{L_{[\text{O III}], \text{narrow}}}{\text{erg/s}}\right) \quad (5)$$

. Meanwhile, bottom panel of Fig. 6 shows the width correlation between the core components and the extended components of the [O III] lines. There is one strong linear correlation with the Spearman Rank correlation coefficient of 0.63. And based on the more recent LTSR technique with considerations of the uncertainties in both coordinates, the strong linear correlation can be described by

$$\log\left(\frac{\sigma_{[\text{O III}], \text{ext}}}{\text{erg/s}}\right) = (0.628 \pm 0.087) + (0.92 \pm 0.04) \times \log\left(\frac{\sigma_{[\text{O III}], \text{narrow}}}{\text{erg/s}}\right) \quad (6)$$

. The strong linear correlations shown in Fig. 6 strongly indicate that the extended components should be not from radial flows in the common [O III] emission line clouds.

Besides, we simply discuss the probable locations of the ex-

tended components of the [O III] lines. The wider extended components (mean second moment of about 500 km/s) can be not broadened by commonly applied broadening techniques for narrow forbidden emission lines. Another technique should be considered. As discussed in Peterson et al. (2013), the gravity influence radius of central supermassive black hole could be about  $\frac{G \times M_{\text{BH}}}{\sigma_{\star}^2}$ , where  $\sigma_{\star}$  represents stellar velocity dispersion in host galaxy. After checking of the SDSS provided stellar velocity dispersions of Type-2 AGN in main galaxies, the common stellar velocity dispersions are about 100-200 km/s in host galaxies of AGN. Therefore, the gravity of central supermassive black holes could affect emission line clouds with distance about several pcs to central black holes with BH masses of about  $10^8 M_{\odot}$ . Then, with consideration of virial effects of gravity of central black holes, the broader extended components could be naturally accepted, if the extended components were from regions more nearer to central black holes. Moreover, the locations of the extended components nearer to central black holes can be naturally applied to explain why part of QSOs without observed extended components of [O III] lines, due to more higher electron density in the clouds nearer to central regions than the critical density for [O III] forbidden line. Moreover, among the 708 QSOs with their [O III] $\lambda 5007\text{\AA}$  well described by two components, 608 QSOs have the blue-shifted extended components. Therefore, the shifted broad extended components are preferred to be from outflows in [O III] clouds more nearer to central black holes, than from the common [O III] line clouds.

Last but not the least, we try to simply but reasonably explain the reported different correlations with different scatters in Fig. 5, through effects of dust extinctions. Without dust extinctions, we assumed that the intrinsic values (marked by the suffix of 'int') follows the linear relations of  $\log(L_{(5100\text{\AA}, \text{int})}) \propto \log(L_{([O \text{ III}], \text{ext}, \text{int})}) \propto \log(L_{([O \text{ III}], \text{narrow}, \text{int})})$ . After extinctions by dusts in the BLRs which only affects the central AGN continuum emissions, in the region between the BLRs and the NLRs and in the NLRs, effects of the dusts on the observed values (marked by the suffix of 'obs') should be

$$\begin{aligned} L_{(5100\text{\AA}, \text{obs})} &= L_{(5100\text{\AA}, \text{int})} \times D_{(\text{BLRs} + \text{ext} + \text{NLRs})} \\ L_{([O \text{ III}], \text{ext}, \text{obs})} &= L_{([O \text{ III}], \text{ext}, \text{int})} \times D_{(\text{ext} + \text{NLRs})} \\ L_{([O \text{ III}], \text{narrow}, \text{obs})} &= L_{([O \text{ III}], \text{narrow}, \text{int})} \times D_{\text{NLRs}} \end{aligned} \quad (7)$$

, where  $D_{(\text{BLRs} + \text{ext} + \text{NLRs})}$ ,  $D_{(\text{ext} + \text{NLRs})}$  and  $D_{\text{NLRs}}$  represents effects of dusts in all regions, effects of dusts in the regions from the BLRs to the observer and the effects of dusts in the NLRs, respectively. Effects of dust extinctions can be considered as the role factor to determine the scatters of the correlations shown in Fig. 5. There are more similar dust extinctions on  $L_{(5100\text{\AA}, \text{obs})}$  and on  $L_{([O \text{ III}], \text{ext}, \text{obs})}$ , but more different dust extinctions on the  $L_{(5100\text{\AA}, \text{obs})}$  and on the  $L_{([O \text{ III}], \text{narrow}, \text{obs})}$ . Therefore, there are tighter correlation between  $L_{(5100\text{\AA}, \text{obs})}$  and  $L_{([O \text{ III}], \text{ext}, \text{obs})}$ , than the correlation between  $L_{(5100\text{\AA}, \text{obs})}$  and  $L_{([O \text{ III}], \text{narrow}, \text{obs})}$ .

Moreover, with considerations of dependence of Balmer decrements (which can be used to trace the dust extinctions) on [O III] luminosity, the steeper correlation of  $L_{(5100\text{\AA}, \text{obs})}$  and  $L_{([O \text{ III}], \text{ext}, \text{obs})}$  can also be simply explained as follows. Based on the observed  $L_{([O \text{ III}], \text{narrow}, \text{obs})}$  and the Balmer decrements from common NLRs  $BD_{(\text{obs}, \text{NLRs})}$  for our objects with both narrow H $\alpha$  and narrow H $\beta$ , we can find there is a moderately negative correlation shown in Fig. 7, with Spearman rank correlation coefficient of about -0.32 with  $P_{\text{null}} \sim 5 \times 10^{-8}$ . And the anti-correlation can be simply described by  $BD_{(\text{obs}, \text{NLRs})} \propto L_{([O \text{ III}], \text{narrow}, \text{obs})}^{-\alpha_{\text{narrow}}}$  with  $\alpha_{\text{narrow}} \sim 0.045$ . Then, combining with the empirical equation to

estimate color excess  $E(B - V) \sim 2 \times \log\left(\frac{BD_{(\text{obs}, \text{NLRs})}}{3.1}\right)$  with 3.1 as the intrinsic flux ratio of narrow H $\alpha$  to narrow H $\beta$ , the intrinsic luminosity  $L_{([O \text{ III}], \text{narrow}, \text{int})}$  can be estimated by

$$\begin{aligned} L_{([O \text{ III}], \text{narrow}, \text{int})} &= L_{([O \text{ III}], \text{narrow}, \text{obs})} 10^{0.4k_{\lambda} E(B-V)} \\ &= L_{([O \text{ III}], \text{narrow}, \text{obs})} \left(\frac{BD_{(\text{obs}, \text{NLRs})}}{3.1}\right)^{0.8k_{\lambda}} \\ &\propto L_{([O \text{ III}], \text{narrow}, \text{obs})}^{(1-0.8k_{\lambda}\alpha_{\text{narrow}})} = L_{([O \text{ III}], \text{narrow}, \text{obs})}^{(1-\beta_{\text{narrow}})} \end{aligned} \quad (8)$$

, where  $k_{\lambda}$  and  $E(B - V)$  represent the reddening curve and color excess, respectively, and  $\beta_{\text{narrow}} = 0.8k_{\lambda}\alpha_{\text{narrow}}$ . Meanwhile, similar equations to estimate intrinsic  $L_{(5100\text{\AA}, \text{int})}$  and intrinsic  $L_{([O \text{ III}], \text{ext}, \text{int})}$  can be described by

$$\begin{aligned} L_{(5100\text{\AA}, \text{int})} &\propto L_{(5100\text{\AA}, \text{obs})}^{(1-\beta_{5100\text{\AA}})} \\ L_{([O \text{ III}], \text{ext}, \text{int})} &\propto L_{([O \text{ III}], \text{ext}, \text{obs})}^{(1-\beta_{\text{ext}})} \end{aligned} \quad (9)$$

, where  $\beta_{\text{ext}} = 0.8k_{\lambda}\alpha_{\text{ext}}$  and  $\beta_{5100\text{\AA}} = 0.8k_{\lambda}\alpha_{5100\text{\AA}}$  have probably different values of  $\alpha_{\text{ext}}$  and  $\alpha_{5100\text{\AA}}$  from the value of  $\alpha_{\text{narrow}}$ , because of different dust obscurations for observed continuum luminosity and for observed luminosity from the extended components of [O III] lines. And, the values of  $\beta$  must be smaller than 1, otherwise an unreasonable result can be expected that intrinsic luminosity after considerations of dust extinctions could be smaller than the observed luminosity. Then, we have the following subequations

$$\begin{aligned} \log(L_{(5100\text{\AA}, \text{obs})}) &\propto \log(L_{([O \text{ III}], \text{ext}, \text{obs})}) \frac{1 - \beta_{\text{ext}}}{1 - \beta_{5100\text{\AA}}} \\ \log(L_{(5100\text{\AA}, \text{obs})}) &\propto \log(L_{([O \text{ III}], \text{narrow}, \text{obs})}) \frac{1 - \beta_{\text{narrow}}}{1 - \beta_{5100\text{\AA}}} \\ \log(L_{([O \text{ III}], \text{ext}, \text{obs})}) &\propto \log(L_{([O \text{ III}], \text{narrow}, \text{obs})}) \frac{1 - \beta_{\text{narrow}}}{1 - \beta_{\text{ext}}} \end{aligned} \quad (10)$$

. Based on the third subequation in Equation (10) combining with the shown results in top panel of Fig. 6, we can find that  $\frac{1 - \beta_{\text{narrow}}}{1 - \beta_{\text{ext}}} \sim 0.83$ . Therefore, the correlation of  $L_{(5100\text{\AA}, \text{obs})}$  versus  $L_{([O \text{ III}], \text{ext}, \text{obs})}$  is steeper, because of its larger slope of  $\frac{1 - \beta_{\text{ext}}}{1 - \beta_{5100\text{\AA}}}$  about 1.2 times larger than the slope of  $\frac{1 - \beta_{\text{narrow}}}{1 - \beta_{5100\text{\AA}}}$  for the correlation of  $L_{(5100\text{\AA}, \text{obs})}$  versus  $L_{([O \text{ III}], \text{narrow}, \text{obs})}$ . Certainly, the results above are highly idealized, and seriously depends on physical properties of dusts in central regions of AGN, however, the results can be applied to find qualitative explanations to the results shown in Fig. 5.

Before the end of the section, we show our simple discussions on which component is well applied to trace central AGN intrinsic luminosity in Type-2 AGN (AGN without observed broad emission lines). Based on the Unified Model for different kinds of AGN (Antonucci 1993; Bianchi et al. 2012; Netzer 2015), central regions of Type-2 AGN are seriously obscured by surrounding dust torus. Therefore, in Type-2 AGN, the extended components of [O III] lines could be totally/partly obscured by dust torus, which indicate the luminosity from the core components could be better applied to trace central AGN intrinsic luminosity, rather the luminosity from the total [O III] lines and from the extended components.

## 4 CONCLUSIONS

Finally, we give our main conclusions as follows. First and foremost, based on the large sample of QSOs with the reliable measured parameters of the [O III] lines including the core components and the extended components and the AGN continuum luminosity, we

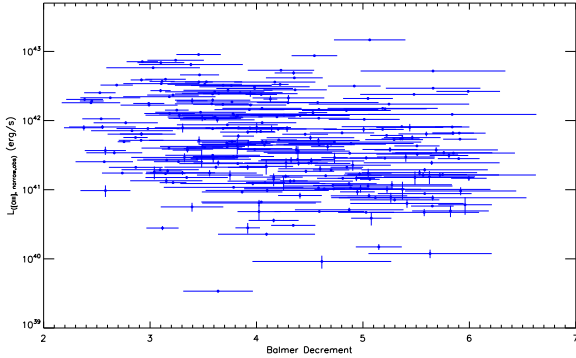


**Figure 7.** Correlation between observed balmer decrements ( flux ratio of narrow  $H\alpha$  to narrow  $H\beta$ ) and the luminosities of the core components of the  $[O\ III]$  emission lines.

check the correlations of  $L_{[O\ III]} - L_{5100\text{\AA}}$ ,  $L_{[O\ III],\ narrow} - L_{5100\text{\AA}}$  and  $L_{[O\ III],\ ext} - L_{5100\text{\AA}}$ , and confirm that the luminosity from the extended components of the  $[O\ III]$  lines leads to more stronger and more tighter correlation. Besides, we confirm the width correlation and line luminosity correlation between the core components and the extended components of the  $[O\ III]$  lines of the QSOs. The results strongly indicate that the extended components are not due to radial flows in common  $[O\ III]$  line clouds, but from radial flows in  $[O\ III]$  clouds more nearer to central black holes. And the wider extended components could be naturally explained by virial effects of gravity of central black holes. Last but not the least, due to probably partly/totally obscured extended components of  $[O\ III]$  lines, the luminosity from the core components should be better applied to trace central AGN intrinsic luminosity in the Type-2 AGN.

## ACKNOWLEDGEMENTS

Zhang and FLL gratefully acknowledge the anonymous referee for giving us constructive comments and suggestions to greatly improve our paper. Zhang acknowledges the kind support from the Chinese grant NSFC-U1431229. FLL is supported under the NSFC grants 11273060, 91230115 and 11333008, and State Key Development Program for Basic Research of China (No. 2013CB834900 and 2015CB857000). This manuscript has made use of the data from the SDSS projects. The SDSS-III web site is <http://www.sdss3.org/>. SDSS-III is managed by the Astrophysical Research Consortium for the Participating Institutions of the SDSS-III Collaboration including University of Arizona, Brazilian Participation Group, Brookhaven National Laboratory, Carnegie Mellon University, University of Florida, French Participation Group, German Participation Group, Harvard University, Instituto de Astrofísica de Canarias, Michigan State/Notre Dame/JINA Participation Group, Johns Hopkins University, Lawrence Berkeley National Laboratory, Max Planck Institute for Astrophysics, Max Planck Institute for Extraterrestrial Physics, New Mexico State University, New York University, Ohio State University, Pennsylvania State University, University of Portsmouth, Princeton University, Spanish Participation Group, University of Tokyo, University of Utah, Vanderbilt University, University of Virginia, University of Washington, and Yale University.

## REFERENCES

- Alam S., et al., 2015, *ApJS*, 219, 12  
 Antonucci R., 1993, *ARA&A*, 31, 473  
 Bennert N., Falcke H., Schulz H., Wilson A. S., Wills B. J., 2002, *ApJL*, 574, 105  
 Bennert N., Jungwiert B., Komossa S., Haas M., Chini R., 2006, *A&A*, 446, 919  
 Bentz M. C., et al., 2013, *ApJ*, 767, 149  
 Berney S., et al., 2015, *MNRAS*, 454, 3622  
 Bianchi S., Maiolino R., Risaliti G., 2012, *Advances in Astronomy*, 2012, 17  
 Boroson T. A. & Green R. F., 1992, *ApJS*, 80, 109  
 Cappellari M., et al., 2013, *MNRAS*, 432, 1709  
 Fischer T. C., Crenshaw D. M., Kraemer S. B., Schmitt H. R., 2013, *ApJS*, 209, 1  
 Greene J. E. & Ho L. C., 2005, *ApJ*, 627, 721  
 Greene J. E., Zakamska N. L., Ho L. C., Barth A., 2011, *ApJ*, 732, 9  
 Hainline K. N., Hickox R., Greene J. E., Myers A. D., Zakamska N. L., 2013, *ApJ*, 774, 145  
 Hainline K. N., Hickox R. C., Greene J. E., Myers A. D., Zakamska N. L., Liu G. L., Liu X., 2014, *ApJ*, 787, 65  
 Heckman T. M., Miley G. K., van Breugel W. J. M., Butcher H. R., 1981, *ApJ*, 247, 403  
 Heckman, T. M., Kauffmann G., Brinchmann J., Charlot S., Tremonti C., White S., 2004, *ApJ*, 613, 109  
 Heckman T. M., Ptak A., Hornschemeier A., Kauffmann G., 2005, *ApJ*, 634, 161  
 Heckman T. M. & Best P. N., 2014, *ARA&A*, 52, 589  
 Kauffmann G., et al. 2003, *MNRAS*, 346, 1055  
 Kovacevic J., Popovic L. C., Dimitrijevic M. S., 2010, *ApJS*, 189, 15  
 Lamastra A., Bianchi S., Matt G., Perola G. C., Barcons X., Carrera F. J., 2009, *A&A*, 504, 731  
 Liu G. L., Zakamska N. L., Greene J. E., Nesvadba N. P. H., Liu X., 2013, *MNRAS*, 430, 2327  
 Liu G. L., Zakamska N. L., Greene J. E., 2014, *MNRAS*, 442, 1303  
 Mateos S., et al., 2016, *ApJ*, 819, 166  
 Marinucci A., Bianchi S., Nicastro F., Matt G., Goulding A. D., 2012, *ApJ*, 748, 130  
 Mullaney J. R., Alexander D. M., Fine S., Goulding A. D., Harrison C. M., Hickox R. C., 2013, *MNRAS*, 433, 622  
 Nelson C. H. & Whittle M., 1996, *ApJ*, 465, 96  
 Netzer H. & Laor A., 1993, *ApJ Letter*, 404, 51  
 Netzer H., Mainieri V., Rosati P., Trakhtenbrot B. 2006, *A&A*, 453, 525  
 Netzer H., 2015, *ARA&A*, 53, 365  
 Oh K., et al., 2015, *ApJS*, 219, 1  
 Peterson B. M., et al., 2004, *ApJ*, 613, 682  
 Peterson B. M., et al., 2013, *ApJ*, 779, 109  
 Reyes R., et al., 2008, *AJ*, 136, 2373  
 Schmitt H. R., Donley J. L., Antonuci R. R. J., Hutchings J. B., Kinney A. L., Pring J. E., 2003, *ApJ*, 597, 768  
 Schneider D. P., et al., 2010, *ApJ*, 139, 2360  
 Shao L., Kauffmann G., Li C., Wang J., Heckman T. M., 2013, *MNRAS*, 436, 3451  
 Shen Y., et al., 2011, *ApJS*, 194, 45  
 Simpson C. 1998, *MNRAS Letter*, 297, L39  
 Stern J. & Laor A., 2012, *MNRAS*, 426, 2703  
 Trouille L. & Barger A. J., 2010, *ApJ*, 722, 212  
 Ueda Y., et al., 2015, *ApJ*, 815, 1  
 Woo J. H., Bae H. J., Son D. H., Karouzos M., 2016, *ApJ*, 817, 108  
 Zakamska N. L., et al., 2003, *AJ*, 126, 2125  
 Zakamska N. L. & Greene J. E., 2014, *MNRAS*, 442, 784  
 Zhang X. G. & Feng L. L., 2016, *MNRAS*, 457, 3878

This paper has been typeset from a  $\text{\TeX}/\text{\LaTeX}$  file prepared by the author.